Phonon-Assisted Second Harmonic Generation in $As_{1-x}Bi_xTe_3-CaBr_2-PbBr_2$ Glasses

I. V. Kityk* and B. Sahraoui

Laboratoire POMA UMR CNRS 6136, Universite d'Angers, Bd Lavoisier 2, Angers, France

Received: August 5, 2004; In Final Form: November 10, 2004

We have found experimentally the IR-induced second harmonic generation (SHG) in glasses possessing different degrees of electron−phonon interactions. For the investigations, we have chosen $As_{1-x}Bi_xTe_3-CaBr_2-PbBr_2$ ($0 < x < 1$) glasses. General formalism is based on consideration of fifth-order nonlinear optical susceptibility. The effect is observed in the middle IR region (spectral range 0.92−10.5 μm) where the value of the electronic energy gap is commensurable to the energies of actual quasi-phonons participating in the anharmonic (noncentrosymmetric) electron−phonon interactions. Varying the As/Bi ratio allows us to operate by the degree of electron−phonon anharmonicity in a wide spectral range. The second harmonic generation (SHG) output signal shows a correlation with IR-induced anharmonic phonon modes within the 1.5−4.8 μm spectral range. A maximum value of SHG is achieved at pump−probe delaying times of about 12.5−20 ps, which are typical for relaxation of the anharmonic electron−quasi-phonon subsystem. The maximally achieved value of the phonon-assisted optical susceptibility was about 6×10^{-38} m^4/V.[4] The SHG signal was saturated for the IR pump power densities of about 1.73 GW/cm^2, corresponding to output SHG signals of about 9.8×10^{-4} with respect to the fundamental ones. By varying the degree of electron−phonon anharmonicity and changing content of glasses, it was unambiguously shown that the IR-induced SHG signal correlates well with changes of oscillator strengths of IR-induced anharmonic phonon modes.

1. Introduction

Generally, second-order nonlinear optical effects in amorphous disordered materials (like glasses, polymers, composites, etc.) are forbidden by symmetry.[1] To induce charge density noncentrosymmetry, an external electric field is usually applied (for example, electroinduced second harmonic generation).[2] Unfortunately, this one is not appropriate for narrow-band IR materials possessing high electroconductivity. At the same time, disordered materials and particularly glasses cause increasing interest due to possible application as materials for IR quantum electronic devices.[3]

IR optical phototreatment[4] in glasses has many attractive applications, because it offers a possibility of production IR-operated waveguides for recording, transformation, and transmittance of IR laser signals possessing different power densities. Now, most of the investigations including all-optical poling were performed for near-IR (less than 2 μm) wavelengths.[3,5,6] Usually, chalcohalide and chalcogenide materials[7−9] have substantial advantages compared to other optical materials, because they have good transparency as well as photo- and thermomechanical stability. Second-order optical effects for such glasses are well-studied for the visible and near-IR spectral ranges.[9] Physical insight of the photoinduced second-order optical properties is significantly different for the middle-IR spectral range compared to the visible and near-IR ones. For this spectral range, we have very close values of electronic band gap of the glasses[8,7] and actual laser-generated IR spectral energies. Because of large laser power densities, one can expect significant contribution of IR-induced anharmonic electron−phonon modes to second-order optical susceptibilities.[8]

The anharmonic electron−phonon interaction (AEPI) is quantitatively described by the third-order space derivative of the electrostatic potential[10] and appears to be crucial at IR-inducing power densities beginning from 0.3 to 0.4 GW/cm^2. In this case, the second-order optical effects might be significant.[11] Both the AEPI as well as second-order optical effects (like the SHG) are described by polar third-rank tensors, and phenomenological description of the observed phenomenon should be similar.

In consideration of second-order optical effects in semiconductors (dielectrics) with energy gaps larger than 1 eV, there exists a relatively large difference between the values of electronic energy gaps and spectral energies of phonon or quasi-phonon (in the case of the disordered materials; however in the article for convenience, we will use the term phonons instead of quasi-phonons) density of states. The role of the photoinduced phonons (due to nonresonant electrostriction-piezoelectric effects) may be described within a framework of perturbation theory,[7−9] and we deal only with low-frequency or static polarization.

The situation becomes qualitatively different when we deal with optically induced phonons possessing energies close to electronic band energy gaps (case of narrow-band semiconductors).[11] In this case, cascading virtual multiphoton processes are not associated only with pure virtual electronic transitions, but possess substantial electron−phonon admixtures[7,8] including additional relaxors. Because of sufficient power IR-induced polarized light in narrow-band semiconductors, there occur IR-stimulated phonons which energies close to electronic interband transitions. In this case, virtual photon−phonon processes of higher order begin to play a substantial role. Because of such kinds of interactions under the influence of external IR-electromagnetic waves, there may occur an anharmonic modulated electron charge density possessing nonzero macroscopic

* University of Physics, J.Dlugosz University of Czestochowa, Al. Armii Krajowej 13/15, Czestochowa, Poland. E-mail: i.kityk@ajd.czest.pl.

10.1021/jp046488y CCC: $30.25
Published on Web 01/22/2005

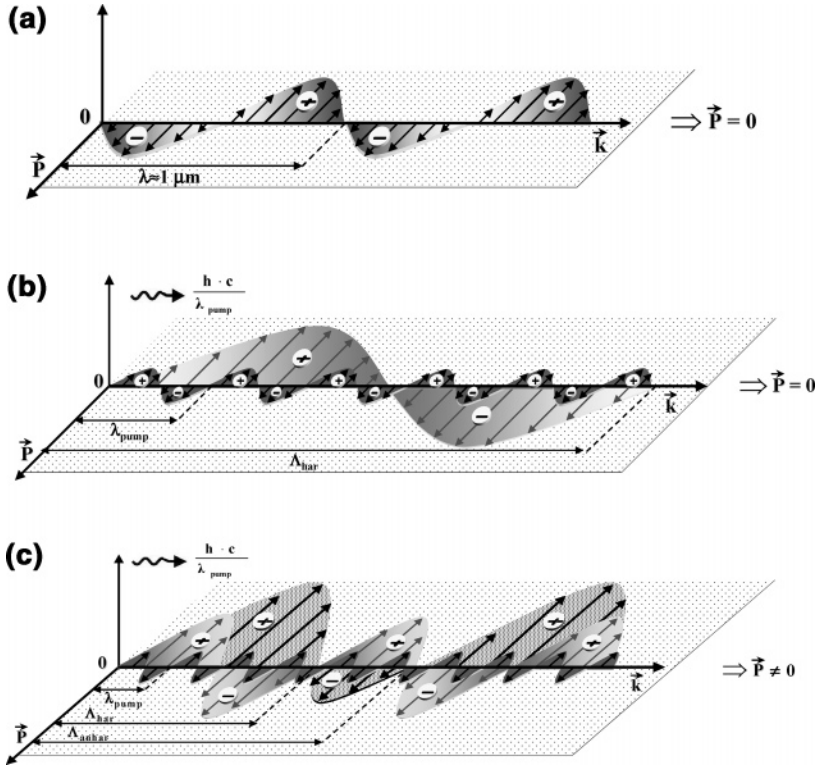

Figure 1. Principal scheme clarifying demonstration of an occurrence of the medium non-centrosymmetry: (a) pure electronic contribution, (b) contribution of one- and two-phonon interaction, (c) contribution of three phonons corresponding to anharmonic electron−phonon interactions.

polarization.[7,8] This is in contradiction to the pure electric polarization disturbed even by harmonic electron−phonon interactions, which should give total macroscopic polarization equal to zero.[7,8]

Appearance of non-centrosymmetric space charge density distribution requires participation of at least three phonons. Contribution of one or two phonons leads to the occurrence of polarization of the medium, in which positive and negative components are compensated, giving the total of zero medium polarization. For clarification, we present in Figure 1 the principal scheme of charge density distribution in the IR-treated medium for different types of interactions. One can see that the pump electromagnetic wave itself should give a self-compensated contribution to the total macroscopic polarization with different signs (see Figure 1a). Inclusion of one or two additional phonons leads to additional modulations of charge density amplitude. However, it will also be compensated, giving the output of zero polarization of the medium (Figure 1b). Only the inclusion of three phonons will be able to cause nonzero medium polarization (Figure 1c). Physically, it means anharmonic electron−phonon interaction described by a third-order tensor, and the efficiency of this process should be dependent on the pump power densities.

The scheme presented in Figure 1 clearly shows that taking into account only electron and harmonic electron−phonon interactions can cause only equilibrium sign distribution of the medium polarization. So, the total polarizability will be compensated, suppressing the nonlinear optical effects described by third-rank polar tensors. Because of sufficient light powers (about 0.1 GW/cm^2), the processes of creation of anharmonic phonons here begin to play a dominant role. Because the processes are determined by a third space derivative of the electrostatic potential, they should favor the occurrence of noncompensated total polarizability, which is responsible for the local noncentrosymmetry, which is necessary for observation of the second-order optical effects. The amplitude of such phonon-assisted non-centrosymmetry will be proportional to the degree of electron−phonon anharmonicity of the given material.

In particular, polarized IR light will cause displacements of particular ions from the equilibrium positions. For the higher IR power densities, this field will cause anharmonic phonon mode bearing. Because of acentric features of the AEPI, IR-induced polarization of the medium will not be fully compensated, giving nonzero total polarization. This value should be higher for the more acentric charge density distribution.

Phenomenologically, the IR-induced SHG effect may be described by an equation

$$P_i = \chi_{ijklmn} E_j^{\omega} E_k^{\omega} E_l^{\Omega_1} E_m^{\Omega_2} E_n^{\Omega_3} \quad (1)$$

where $E_{l,m,n}^{\Omega_{1,2,3}}$ are effective electric strengths created by the phonon displacement fields, particularly due to IR-induced electrostriction and piezoelectric effects.

In the present paper is proposed a kind of IR optical poling consisting of IR-photopumping of appropriate electronic and phonon states using pulsed-IR parametric generators operating within 3.4−10.7 μm spectral range. It is necessary to emphasize that the observed effect is principally different compared to the all-optical poling,[12] where coherent bicolor interaction is important.

In section 2, the experimental method and corresponding results are presented. Section 3 describes phenomenological and microscopic description of the observed phenomenon.

2. Experimental Method

2.1. Sample Preparation. For the investigation, we have chosen the $As_{1-x}Bi_xTe_3-CaBr_2-PbBr_2$ ($0 < x < 1$) glasses with transparency shown in Figure 2. A specific feature of these glasses consist of the possibility of varying the anharmonic electron−phonon interaction by changing the parameter x, which unambiguously is related to Bi/As ratio.

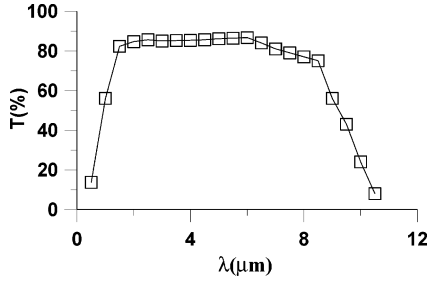

Figure 2. Spectral transmission of $As_{1-x}Bi_xTe_3-CaBr_2-PbBr_2$ glass.

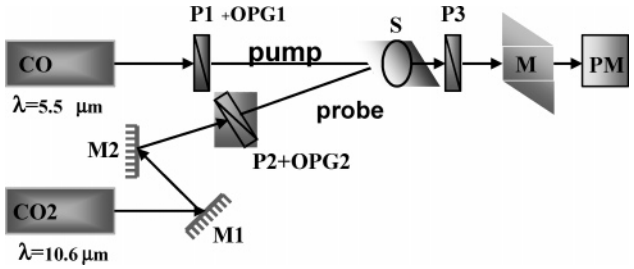

Figure 3. Principal setup for measurement of IR-photoinduced SHG.

The investigated glasses were synthesized from congruent melt by a method similar to that described in refs 8 and 9. The parameter of Bi/As ratio was varied in the ranges 0.22−0.68 and 1.15−1.32. These content ranges correspond to phases of thermodynamically homogeneous glass formation monitored by differential scanning calorimetry (DSC). The $CaBr_2$ compound favors the glass-forming tendency of the considered system. Without the $PbBr_2$, one cannot form bulk glass because of the higher field strength of the Pb^{2+} ion. The sample's homogeneity determined by X-ray diffraction and optical polarized methods was about 3.4%. The samples investigated were in the form of parallelepipeds with sizes of about $5 \times 5 \times 0.8$ mm^3. The scattering background was less than 0.25%.

2.2. Experimental Setup. The experimental setup is presented in Figure 3. The pulsed CO laser (CO) beam ($\lambda = 5.5$ μm; $P = 10-22$ MW; $\tau = 0.44-80$ ps; frequency repetition of 8−15 Hz) serves as an IR pump beam and together with a system of polarizer and optical parametrical proustite generators (P1 + OPG1) allows the reception of a quasi-continuous generation within the 2.0−6.05 μm spectral range. A picosecond mode-locked CO_2 laser (CO2) beam ($\lambda = 10.6$ μm; $P = 25$ MW; $\tau = 2-10$ ps) together with a set of Zn(Se, Te) optical parametrical generators (P2 + OPG2) is used as a probing (fundamental) beam generating within the range 4−11 μm. The setup allows the variation of wavelengths of both the pump and probing laser beams. The fundamental and probing laser beams were temporarily synchronized, and additional delaying line was used for the creation of pump−probe retardation.

An IR-cooled fast-response photomultiplier (PM) registered an illumination passed through grating monochromator M with spectral resolution of about 8 nm/mm. The PM output was connected with an electronic boxcar integrator (gain time up to 420 ps), which was applied for detection of the SHG output signal at different incident angles of the fundamental beam.[18] Maker fringence experimental technique[19] was applied for determination of the output SHG signal. Evaluations of the second-order optical susceptibilities were performed by a method described in ref 13.

Photoinduced birefringence was determined by the Senarmont method for correct evaluation of the photoinduced phase-matching renormalization. The setup allows one to perform the measurements for both the varied and fixed wavelengths of pumping and fundamental laser beams, contrary to our earlier works,[9] where the measurements were done at fixed pumping and probing wavelengths.

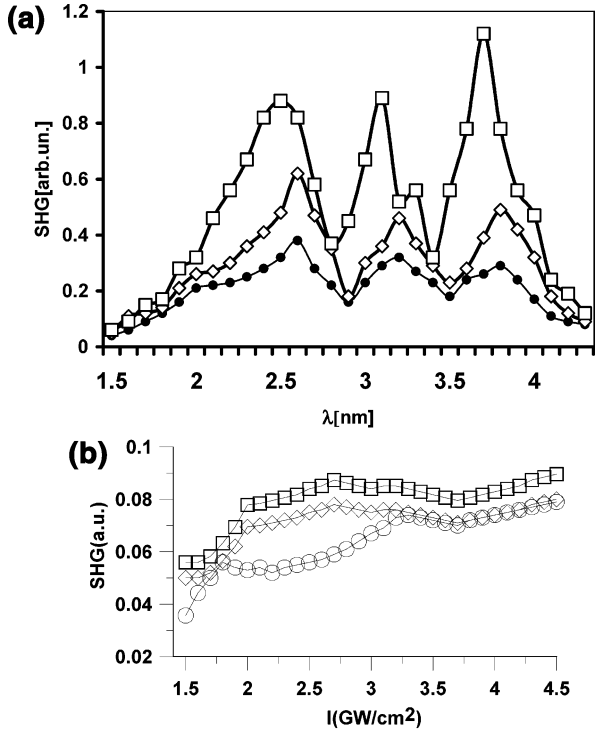

Figure 4. (a) Spectral dependencies of the SHG output signal (proportional to $\chi^{(2\omega)}$) at the fixed pump power density of 1 GW/cm^2 at different wavelengths of the pumping beams: circles, 4.5 μm; rhombs, 3.5 μm; squares, 2.7 μm for As/Bi = 1.21. (b) Spectral dependencies of the SHG output signal (proportional to $\chi^{(2\omega)}$) at the fixed pump power density of 1 GW/cm^2 at different wavelengths of the pumping beams: circles, 4.5 μm; rhombs, 3.5 μm; squares, 2.7 μm for As/Bi = 0.50.

Angles between the pump and probe laser beams have been varied within the range 12−36°. Polarizations of the pump, probe, and output SHG beams were defined by polarizers P1, P2, and P3, respectively. The $\chi^{(5)}$ tensor values were evaluated by the accounting of Fresnel losses, Gaussian-like sequence of the beam profile, optical attenuation, and the photoinduced birefringence. A parasitic fluorescence signal was observed below 1.22 μm, which corresponds to emission from the trapping intraband levels. This allowed one to spectrally separate the doubled frequency SHG output signal from the scattering noise using a grating monochromator (M) with spectral resolution of about 7 nm/mm. The proper time duration of the SHG signal was about 1.2−1.4 ps.

3. Experimental Results

In Figure 4a−b, spectral dependencies of the IR-stimulated SHG output signal (proportional to $\chi^{(2\omega)}$) at the fixed pump IR-power density (about 1 GW/cm^2) are given for different pump wavelengths. We have chosen the pump wavelengths at near-IR resonances ($\lambda = 2.7$, 3.5 μm) and outside the resonance spectral range (4.5 μm). The investigations were done for the samples possessing different As/Bi ratios (compare Figure 4a and b) for the same pump−probe conditions. Quantitatively, parameters of the degree of the AEPI were estimated as third-order space derivatives of electrostatic potential within the particular structural clusters. Our evaluations performed by the norm-conserving pseudopotential method[8,14−16] have shown that maximal variations of the AEPI exist for As−Bi(Te) clusters,

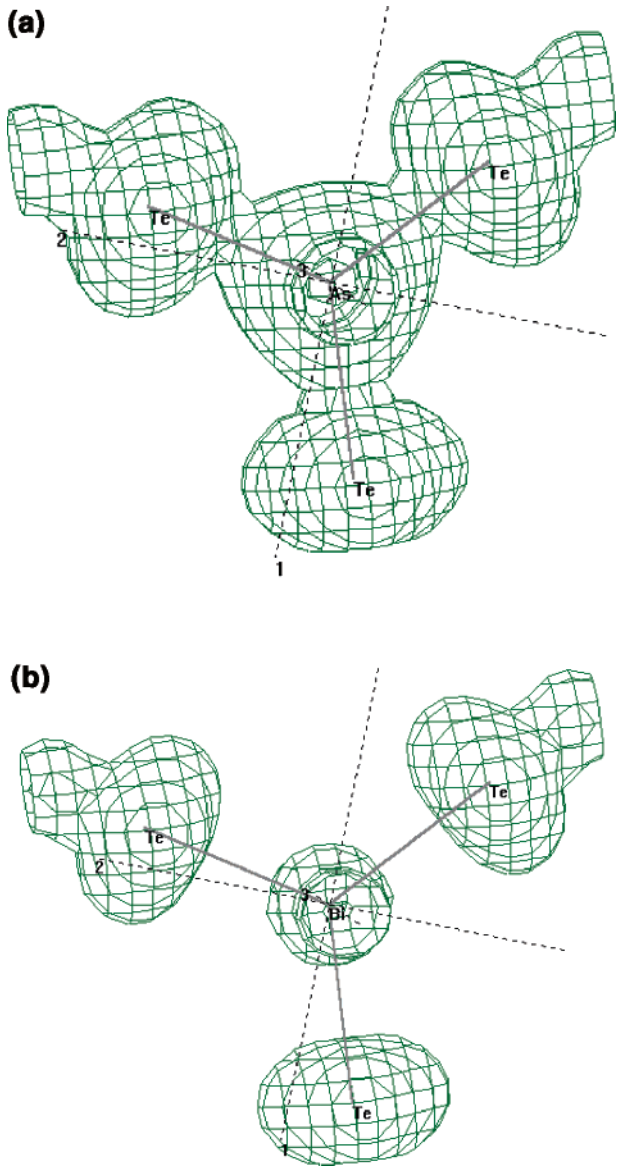

Figure 5. Effective charge density distribution within the Bi(As)−Te cluster with e/Ω = 0.1 e/A^3: (a) a case of Bi cationic atoms, (b) case of As cationic atoms.

varying from 0.086 eV/A^3 (As/Bi = 0.46) up to 0.72 eV/A^3 (As/Bi = 1.21). It may be clearly demonstrated by the calculated quantum-chemically charge density distribution for the two limiting cases (possessing As and Bi as principal cationic atoms) (see Figure 5). Taking into account a superposition of external glass background, one can see that the replacement of Bi by As should lead to substantial changes of the electrostatic potential gradients and of the corresponding AEPI. From Figure 5, one can clearly see that the space charge density distribution is very sensitive to the replacement of Bi by As and should lead to substantial changes of third-order space derivatives defining the AEPI. So, by varying the As/Bi ratio, there exists a possibility to vary the degree of the AEPI.

From Figure 4a, one can see that by successively tuning the pump wave closer to the resonances (3.5 and 2.6 μm) there also appears to be an additional possibility to enhance the SHG. Moreover, we observe clearer spectral SHG modulation (Figure 4a) corresponding to the interband quasi-resonances, which may originate from the enhanced oscillator strength of anharmonic modes with several spectral maxima. The group-theory analysis together with quantum chemical calculations indicate that the

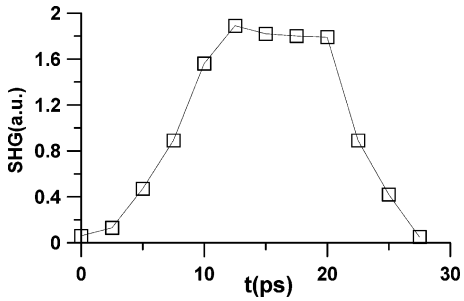

Figure 6. Typical dependence of the IR-induced SHG output signal vs pump−probe delaying time.

TABLE 1: Principal Parameters of the IR-Induced Phonon Modes for As/Bi = 1.21

indication of the peaks	wavelength (μm)	phonon mode 1	phonon mode 2	phonon mode 3
1	2.6 (3810 cm^{-1})	1862 (A1)	974 (B2)	974 (B2)
2	3.12 (3200 cm^{-1})	1201 (A1′)	1289 (A1″)	710 (B1)
3	3.7 (2700 cm^{-1})	1201 (A1′)	1289 (A1″)	210 (B1)

observed phonon modes originated from LO + TO modes of the As−Te−Bi structural fragment described by two 2A1 + B1 noncentrosymmetry and A1 + 2B2 stretching modes corresponding to the C_3 site point group of the As−Te clusters (see Table 1).

The corresponding anharmonic phonon modes should possess wavelengths corresponding to 2.6, 3.12, and 3.7 μm. The observed spectral shift of the SHG compared to the actual phonon modes (up to 0.1 μm) (see Figure 4) may be caused by additional spectral redistribution of the IR-pumping light. Increase of the fixed pump powers causes an increase of the output SHG value. It is necessary to add that at pump power densities below 0.25 GW/cm^2 the IR-induced SHG signal is comparable with the background noise.

Figure 4b has unambiguously shown that material with less anharmonicity (in our case, As/Bi = 0.50) leads to substantially less SHG signal and to the disappearance of resonance-like structure. This may be a confirmation of the dominant role played by AEPI in the observed fifth-order NLO process. It is necessary to emphasize that the IR-induced SHG is enhanced with increasing IR pump power (within the range 0−1.75 GW/cm^2) for all the investigated glasses.

The maximally achieved values of the fifth-order susceptibilities equal to 6×10^{-38} m^4/V.[4] The SHG signal reaches a saturation point for the IR-pumping power densities at about 0.73 GW/cm^2. The values of diagonal tensor component $\chi^{(2\omega)}_{xxxxx}$ is at least one-half an order of magnitude larger than those for the off-diagonal tensor component. A slight photochemical destruction process is observed for pump power densities higher than 1.02 GW/cm^2.

Another important factor confirming the significant role of the AEPI consists of dependence of the SHG intensity versus the pump−probe delaying time (see Figure 6). One can clearly see that the maximum SHG signal is observed for pump−probe delaying times equal to about 13−20 ps, which are typical for relaxation times of the AEPI.[8,9] A specific feature of the pump−probe delay in this case consists of the occurrence of a flat pump−probe-delayed SHG maximum. This behavior is substantially different than the features obtained from static electron−phonon anharmonities.[8,9] This reflects participation of a higher number of effective quasi-phonons giving a contribution to the observed effect. As a consequence, the quasi-phase-matched pump−probe conditions will be realized at higher pump−probe delaying times.

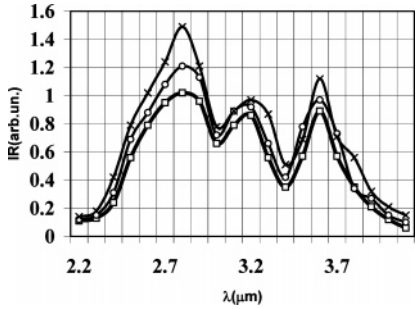

Figure 7. IR-induced spectral dependences of the IR oscillator strengths at different pump powers at $\lambda = 2.7$ μm: □, 0.25 GW/cm^2; ○, 0.50 GW/cm^2; ×, 0.85 GW/cm^2. The IR oscillators are determined from the IR absorption spectra at the same pump conditions as the SHG measurements.

One difference of the noncoherent IR poling compared to the pure coherent optical poling consists of comparable values of IR-induced electronic and phonon (ionic displacement) dipole moments contributing to the nonlinear optical susceptibilities.

The first condition is achieved because of the close values of the IR-induced frequencies and IR energy gaps. The second is caused by the inducement of acentric charge density anisotropy due to IR-induced anharmonic phonons.

Experimentally, the first effect may be manifested through the spectral SHG dependences versus the anharmonic phonon frequencies. The second may be displayed through the monitoring of the pump−probe nonlinear optical kinetics occurring at a delay time of about 20 ps, contrary to the ultrafast pure electronic relaxation time (below 1 ps) in the usual multiphoton processes.

In Figure 7 are shown the changes of IR-induced oscillator strengths obtained from the IR mode maxima (evaluated from IR absorption) at different IR-pump powers. These modes are evaluated from the intensities of the particular IR modes versus photoinduced pump power.

One can observe increasing anharmonic phonon mode strengths, which demonstrate a correlation with intensity dependences of the SHG presented in Figure 4. We have monitored the changes at the same conditions as for the IR pump light excitation.

4. Theoretcal Description and Discussion

Quantum chemical calculations of second-order optical susceptibilities were done to estimate behavior of the SHG for two types of processes: without and with inclusion of the AEPI versus retarding time and pump power following a formalism developed by us previously.[8,9] Calculations were done considering both traditional formalism of second-order susceptibility $\chi_{ijk}^{(2\omega)}$ (pure electronic two-photon cascading processes) as well as higher-order steady-state multiphoton processes.

Following a cluster's self-consistent norm-conserving pseudopotential calculations (for details, see refs 8 and 14−16) within the plane-wave basis set for glasses, we have simulated the spectral behavior of the fifth- and second-order nonlinear optical (NLO) effects. From Figure 8, one can see that only appropriately taking into account the AEPI could give a substantial output SHG signal compared to the pure electronic cascading process. The intensity of the output SHG signal caused only because of pure electronic contribution should be equal to about 10^{-6}−10^{-7} with respect to the fundamental ones. The anharmonic phonon subsystem gives a contribution of at least one order higher, which is actually observed experimentally.

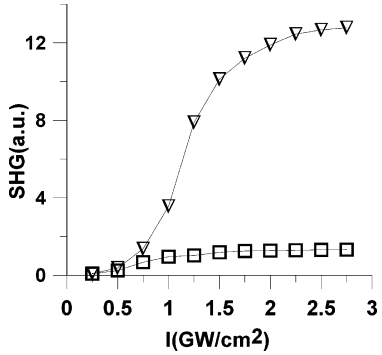

Figure 8. Theoretically simulated dependences of the IR-induced SHG: □, within a framework of traditional second-order processes; ▽, the same with inclusion of the photoinduced anharmonic electron−phonon interactions as described in the paper.

Our calculations were carried out using the quantum chemical computer package *HYPERCHEM 7.0*. They showed that the [Bi−As]−Te chemical bonds play a crucial role in the observed photoinduced nonlinear optical susceptibilities. For Pb−Br and Ca−Br bonds, IR-induced changes are relatively small (less than 1.88%). In particular, the matrix dipole moments for the As−Bi bonds are equal to about 8.76 D . Contribution of Pb−Br and Ca−Br bonds to IR-induced changes are equal to 0.21 and 0.87 D, respectively. The interaction of the fundamental IR laser beam $E_{pr}^{(\omega)}(r, t)$ with the investigated medium may be described as follows:

$$E(r, t) = E_{pr}^{(2\omega)}(r, t) + E_{pr}^{(\omega)}(r, t) + E_{pump}^{(\omega_p)}(r, t) + E^{(\Omega_1 \pm \Omega_2 \pm \Omega_3)}(r, t - \tau) \quad (2)$$

where τ is a pump−probe delay time; the indices pump and pr correspond to pumping and probing IR beams, respectively. The interacting photon effective electric field strengths are presented within the plane-wave approximation

$$\mathbf{E}_{pr}^{(\omega)}(r, t) = \mathbf{E}^{(0)} \exp[i(\omega t + kr + \phi_1)] \quad (3)$$

where $\mathbf{E}^{(0)}$ and ϕ_1 are amplitude and phase of the electromagnetic fundamental wave, respectively, and possess the frequency (ω) at instant time (t) and the point of space ($\mathbf{r}$).

A term with frequency of 2ω is caused by IR-induced noncentrosymmetry and is similar to process with interference of two coherent waves with fundamental and doubled frequencies (optical poling).[17] The temporarily averaged output of nonlinear polarization for the doubled frequency may be expressed in the form

$$P^{(2\omega)}(r) \cong \epsilon_0 |E_{pr}^{(\omega)}(r, t - \tau)|^2 \{\langle E_{pump}^{\omega_p}(r, t) \cdot [E^{\Omega_1 \pm \Omega_2 \pm \Omega_3}(r, t)]^2 \rangle + \langle E_{pr}^{\omega}(r, t) [E^{\Omega_1 \pm \Omega_2 \pm \Omega_3}(r, t)]^2 \rangle \langle E_{pr}^{2\omega}(r, t - \tau) \cdot [E^{\Omega_1 \pm \Omega_2 \pm \Omega_3}(r, t)]^2 \rangle\} \quad (4)$$

where the brackets mean averaging over time.

The first term corresponds to the interaction between the pumping laser beam and the modulated IR-excited noncentrosymmetric charge density distribution due to IR-induced anharmonic displacement phonon modes possessing combined frequencies $n_1\Omega_1 \pm n_2\Omega_2 \pm n_3\Omega_3$**.** The electric field strength amplitudes of the photoinduced anharmonic displacement modes, $[E^{(\Omega_1 \pm \Omega_2 \pm \Omega_3)}(r, t)]$ are proportional to the IR-inducing power density. From general phenomenological consideration, one can conclude that the SHG output will be maximal for

parallel directions of polarization for pumping and fundamental beams. This one reflects a fact that direction of the anharmonic charge density shift should be parallel to the direction of the pumping (IR-induced) beam polarization.

Another requirement is associated with satisfying the phase matching conditions that, in the case of the fifth-order cascading process, are fulfilled in the larger range of angles compared to the traditional second-order SHG. The second-order non-centrosymmetric effect may be observed because there exists a range of phonon frequencies satisfying the conditions $\omega - \omega_1 \pm n\Omega_1 \pm g\Omega_2 \pm h\Omega_3 = 0$ ($n, g, h = \pm 1, \pm 2, \pm 3,...$) which are necessary for the appearance of non-centrosymmetric tensor components during the IR-picosecond photoexcitation and satisfaction of coherent interaction conditions.

For the fifth-order cascading nonlinear interactions, we should consider interactions between the fundamental ($k_{pr}^{(\omega)}$) doubled frequency ($k^{(2\omega)}$), pumping $k_{pump}^{(\omega_p)}$ beams from one side and photoinduced combined IR-induced anharmonic frequencies of the medium with wave vectors ($K^{(\Omega_1 \pm \Omega_2 \pm \Omega_3)}$). As a consequence, we obtain a relatively wide range of angles satisfying the phase matching conditions

$$P^{(2\omega)}(r, t) \cong \epsilon_0 \chi^{(5;\,2\omega)}(2\omega; \omega, \omega, \Omega_1, \Omega_2, \Omega_3)|E_{pr}^{(\omega)}(r, t)|^2 \cdot \exp(-i\Delta k r) \quad (5)$$

where $\Delta k = k^{(2\omega)} - k_{pr}^{(\omega)} \pm [k_{pump}^{(\omega_p)} + K^{(\Omega_1 \pm \Omega_2 \pm \Omega_3)}]$.

The range of angles satisfying phase-matching conditions should be relatively wide, because there exists a large number of phonon modes satisfying these conditions within the spectral range 1.1−6 μm.

5. Conclusions

In the present work, phonon-assisted SHG was experimentally observed in halcohalide $As_{1-x}Bi_xTe_3-CaBr_2-PbBr_2$ glasses. By varying the parameters of the anharmonic electron−phonon interactions by changing As/Bi ratio, we have unambiguously shown that the observed effect is caused by the anharmonic EPI. The main difference of the present cascading fifth-order nonlinear optical effect compared to the traditional second-order one consists of a substantial contribution of anharmonic electron−phonon subsystems induced by the IR pumping power. Independent measurements of the principal photoinduced IR oscillator strengths additionally confirmed a good agreement between spectral positions of the photoexcited IR modes and the output SHG. The relaxation kinetics of these effects is consistent with a simple model of electron−phonon anharmonic interactions.

References and Notes

(1) Bloembergen, N. *Nonlinear Optics*; Benjamin: New York, 1965. Boyd, R. W. *Nonlinear Optics*; Academic: Boston, 1992.
(2) Chemla, D. S.; Zyss, J. *Nonlinear Optical properties of Organic Molecules and Crystals*; Academic: New York, 1986; Vols. 1 and 2.
(3) Qiu, J.; Si, J.; Hirao, K. *Opt. Lett.* **2001**, *26*, 914. Tanaka, K. *Appl. Phys. Lett.* **2002**, *80*, 177.
(4) Gautier, C. A.; Lefumeux, C.; Albert, O.; Etchepare, J. *Opt. Commun.* **2000**, *178*, 217.
(5) Antonyuk, B. P. *Opt. Commun.* **2000**, *181*, 191.
(6) Charra, F.; Kajzar, F.; Nunzi, J. M.; Raimond, F.; Idiart, E. *Opt. Lett.* **1993**, *18*, 941.
(7) Zhao, X.; Xu, L.; Yin, H.; Sakka, S. *J. Non-Cryst. Solids* **1994**, *167*, 70.Kityk, I. V.; Kasperczyk, J.; Plucinski, K. *J. Opt. Soc. Am.* **1999**, *16B*, 1719.
(8) Kityk, I. V.; Sahraoui, B. *Phys. Rev. B* **1999**, *60*, 942.
(9) Sahraoui, B.; Kityk, I. V. *J. Opt. A Pure Appl. Opt.* **2003**, *5*, 174.
(10) Geller, M. R.; Dennis, W. M.; Markel, V. A.; Patton, K. R.; Simon, D. T.; Yang, H. S. *Physica B* **2002**, *316-317*, 430.
(11) Napieralski, J. *Ferroelectrics* **1999**, *220*, 17.
(12) Balakirev, M. K.; Kityk, I. V.; Smirnov, V. A.; Vostrikova, L. I.; Ebothe, J. *Phys. Rev. A* **2003**, *67*, 023806.
(13) Kityk, I. V.; Marciniak, B.; Mefeh, A. *J. Phys. D: Applied Physics* **2001**, *34*, 1.
(14) Davydov, A. S. *Introduction to the Solid State Physics*; Nauka: Moscow, 1997 (in Russian).
(15) Bachelet, G. B.; Hamann, D. R.; Schluter, M. *Phys. Rev.* **1982**, *26B*, 4199.
(16) Sahraoui, B.; Kityk, I. V.; Nguyen Phu, X.; Hudhomme, P.; Gorgues, A. *Phys. Rev.* **1999**, *59B*, 9229.
(17) Etile, A.-C.; Fiorini, C.; Charra, F.; Nunzi, J.-M. *Phys. Rev.* **1997**, *56A*, 3888.
(18) Melancholin, A. *Principles of measurements in the crystallooptics*; Nauka: Moscow, 1974 (in Russian).
(19) Maker, P. D.; Terhune, R. W.; Nisenoff, M.; Savage, C. M. *Phys. Rev. Lett.* **1962**, *8*, 41.